Hindawi
Adsorption Science & Technology
Volume 2021, Article ID 5593245, 15 pages
https://doi.org/10.1155/2021/5593245

Research Article

Micropore Characteristics and Gas-Bearing Characteristics of Marine-Continental Transitional Shale Reservoirs in the East Margin of Ordos Basin

Yuanzhen Ma,[1] **Meng Wang**,[2,3] **Ruying Ma**,[1] **Jiamin Li**,[1] **Asiya Bake**,[1] **and Yadi Shan**[2]

[1]*College of Geology and Mining Engineering, Xinjiang University, Urumqi 830046, China*
[2]*School of Resources and Geosciences, China University of Mining and Technology, Xuzhou 221116, China*
[3]*Jiangsu Key Laboratory of Coal-Based Greenhouse Gas Control and Utilization, China University of Mining and Technology, Xuzhou 221008, China*

Correspondence should be addressed to Meng Wang; wangm@cumt.edu.cn

Received 21 January 2021; Revised 1 April 2021; Accepted 8 May 2021; Published 24 May 2021

Academic Editor: Nguyen Hai Tran

In order to deeply study the exploration potential of Carboniferous-Permian marine-continental transitional shale reservoirs in the Ordos Basin, the shale samples from well Y1 in the central-southern part of the Hedong Coalfield were used as the research object. The organic geochemical test, scanning electron microscope, X-ray diffraction, and high pressure mercury injection and low-temperature nitrogen adsorption experiments have studied the microscopic characteristics and gas content characteristics of shale reservoirs. The results show that the organic matter type of the sample is type III; the TOC content ranges from 0.28% to 16.87%, with an average of 2.15%; R_o is from 2.45% to 3.36%, with an average value of 2.86%; the shale pores in the study area are well developed, containing more organic pores and intergranular pores of clay minerals. Based on the two-dimensional SEM image fractal theory to study different types of pores, the fractal dimension of shale pore fracture morphology is between 2.34 and 2.50, and the heterogeneity is moderate. The high-pressure mercury intrusion experiment characterizes the pore size distribution of shale macropores and transition pores. The pore diameters are mostly nm-scale. Transition pores are the main pores of the shale in the study area. Based on the characteristics of the pore structure, the adsorption capacity and gas content of CH4 in shale reservoir were analyzed by methane isothermal adsorption and gas content experiments. The results showed that the pore volume and specific surface area were positively correlated with clay mineral content, TOC, and RO, but negatively correlated with the quartz content. In clay minerals and brittle minerals, pore volume and specific surface area are positively correlated with illite content and negatively correlated with the quartz and kaolinite content. The measured total gas content and desorbed gas content are significantly positively correlated with TOC, but are weakly positively correlated with the quartz and illite content. This study finely characterizes the physical properties, micropore characteristics, gas-bearing characteristics, and influencing factors of shale reservoirs, which has certain theoretical guiding significance for the research and development of coal-measure shale in the Ordos Basin.

1. Introduction

The Shanxi group of the Upper Permian in the Ordos Basin has developed a set of shallow lake-rich organic shale [1], which has a good prospect for exploration according to the former exploration reality [2–4]. So far, domestic studies on shale gas reservoirs have focused on the marine phase of the Lower Paleozoic boundary in south China, and there have been few studies on the marine-continental transitional shale in North China [5–9], and further discussion is needed on the microscopic characteristics of shale reservoirs and the mechanisms of shale gas endowment and storage.

Yang et al. [10] have studied the microscopic pore types of land-phase shales in the Ordos Basin and their influence

on shale gas storage seepage, Tian et al. [11] have studied the microstructural characteristics of marine and land-transition phase shales in the middle-eastern Qinshui Basin, and Guo et al. [12] have discussed the influencing factors of the reservoir gas content based on the testing of Upper Paleozoic boundary mud shale samples in the Ordos Basin and initially proposed that the Upper Yangzi of China Paleocene shale gas reservoir evaluation program [12, 13]. Xie et al. [14, 15] have carried out an indepth study of the pore structure of marine shales and studied the fractal characteristics using the idea of fractography, and Yang [16] pointed out that organic matter is the main factor affecting the fractal dimension. Previous studies mainly focused on the microscopic characteristics of pores in marine and continental shale gas reservoirs, but relatively, few studies have been conducted on marine-continent transitional coal-measure shale gas reservoirs. Due to the limitations of research precision and complexity, further indepth research is needed on the microscale pore structure, heterogeneity, influencing factors, and the relationship with shale gas geological parameters of shale gas reservoirs.

Some studies have been carried out on the marine-continental transitional shales in Ordos Basin and Lower Yangzi region [17, 18], but the microstructural characteristics of the marine-continental transitional shales in Ordos Basin are relatively weak. In this paper, taking the Y1 well in the middle part of the Hedong coalfield (Figure 1) as an example, the shale reservoir was studied and analyzed from the aspects of reservoir physical properties, organic matter development, rock mineral composition, storage space, and gas content using microscopic analysis, X-ray diffraction, and organic geochemical testing, in order to provide some guidance for evaluating the resource potential of the marine-continental transitional shale reserves in the Ordos Basin.

2. Basic Geology of the Study Area

The Hedong Coalfield is located at the eastern margin of Ordos Basin, adjacent to the Shanxi Massif in the east, and in contact with the Qinling and Yinshan tectonic zones in the north and south, respectively. The study area is located in the south-central part of the Hedong Coalfield. The basic structure of this area was formed in the Mesozoic era, and the tectonic deformation has been weak for a long time, which is a transitional type of basin margin tectonics. It differs both from the Shanxi massif, which is strongly active, and the Ordos basin, which is relatively stable. The east boundary of the Lishi Rift is a north-south tectonic zone, and the west Jinxi uplift zone, mainly the Lvliang dorsal slope, is also north-south oriented; so, the north-south tectonics is the main controlling factor of the tectonic deformation in this area.

The study area passes through the strata of the Fourth Baode group, Jurassic Daitong group, Triassic Yanchang group, Tongchuan group, Ermaying group, Heshanggou group, Liujiagou group, Permian Shiqianfeng group, Upper Shihezi group, Lower Shihizi group, Shanxi group, Carboniferous Taiyuan group, Benxi group, and Ordovician Fengfeng group. The development lithology is mainly sandy mudstone, mudstone, siltstone, siltstone, and so on. The tectonic diagram of this area and the drilling locations are shown in Figure 1.

3. Samples and Testing

3.1. Sample Collection. In this study, with reference to the research results of Dai et al. [19], Xie et al. [20], and Ma et al. [21, 22], the Y1 well was selected as a favorable area for shale gas exploration, and a total of 56 shale samples were collected at different depths from the Lower Shihezi group, Shanxi group, and Taiyuan group in the main mud shale formation, and the samples were numbered from Y1-1 to Y1-56 from shallow to deep.

3.2. Sample Tests. The Shanxi Institute of Coal Geological Exploration was entrusted to detect and analyze the shale reservoir in this area. 56 shale samples were selected for the TOC test, and 7 shale samples were selected for Ro, XRD, SEM, rock pyrolysis, high-pressure mercury injection, and low-temperature N2 adsorption test, including geochemical analysis, petrographic characterization, and reservoir physical properties analysis, and the experiments were conducted in strict accordance with national standards.

3.2.1. Organic Geochemical Characterization Experiments. The total organic carbon content of a total of 56 shale samples was measured using a CS-800 analyzer; the specular body reflectance was measured using a Leica DM4500p polarized light microscope, and the hydrocarbon precipitation and the maximum cracking temperature of the rock pyrolysis experiment were measured using an OG-2000V pyrolyzer at different temperatures.

3.2.2. Lithological Characterization Experiments. The mineralogical characteristics of the mud shale samples were identified by rock flake and Leica DM4500p polarized light microscope according to the technical specification of rock mineral identification; the whole rock and clay mineral composition of the samples were detected by SmartLab X-ray diffractometer; the SEM was pretreated by Tescan/OXFORD scanning electron microscope, and the samples were polished by argon ion before the experiment.

3.2.3. Reservoir Physical Property Characterization Experiments. The reservoir physical property analysis included mercury compression, specific surface area, and gas content tests. Seven representative samples were selected from the Lower Shihezi group, Shanxi group, and Taiyuan group, and their pore networks were finely characterized by high-pressure mercury injection and low-temperature N_2 adsorption, and the pore porosity, specific surface area, pore volume, and pore diameter were measured.

High-pressure mercury piezometry is usually used for macroporous pores, and the Quantachrome Poremaster fully automatic mercury piezometry is used for high-pressure piezometry. For mesoporous pores, the specific surface area and pore size distribution of the pores in the shale were measured by low-temperature nitrogen adsorption using a GEMS V-Sorb 2800TP specific surface area and pore size analyzer. The HT-WB12 thermostatic water bath analyzer was used

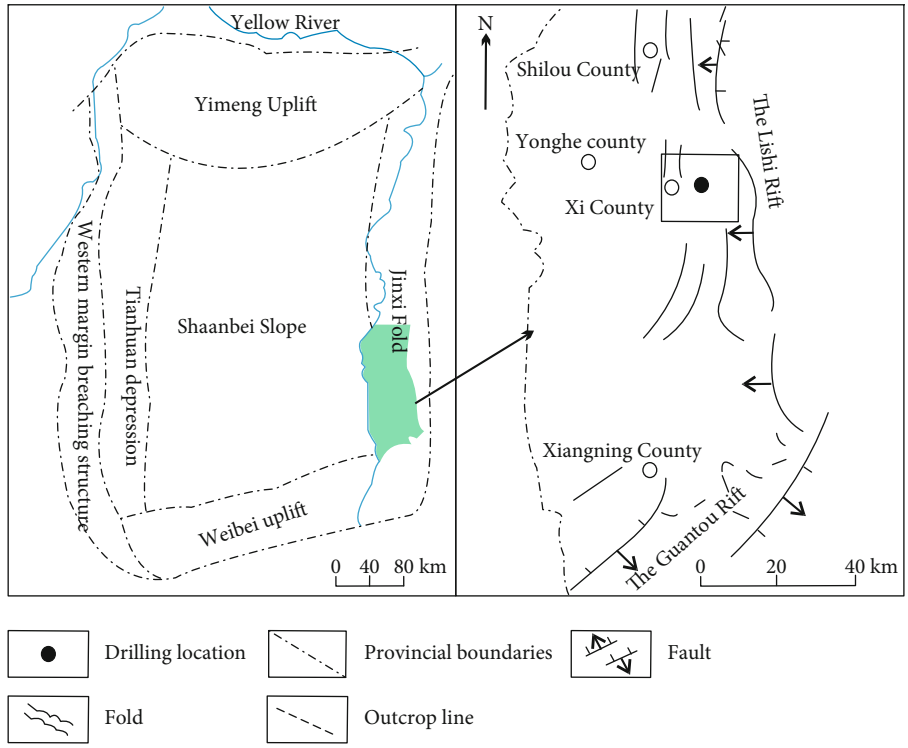

Figure 1: The structural diagram of the study area [19] and the location map of sampling points.

to test the gas content of the target reservoir shale. The above tests were conducted at the Shanxi Coal Geological Exploration Institute.

4. Results

4.1. Organic Geochemical Characteristics. The geochemical parameters of shale samples are shown in Table 1. The organic matter types of shale samples are type III (humic); the TOC content is between 0.28% and 16.87%, with an average of 2.15%, which is higher than the lower limit value of gas-producing shale [23]. The TOC content of Shanxi Formation in the middle part is higher, with an average of 2.92%; the samples with the organic matter content greater than 2.0% reach 46.43% (Figure 2); R_o values ranged from 1.71% to 2.10%, with an average of 1.89%, reaching a high maturity stage, and a large amount of pyrogenic gas has been generated for type III organic materials; $S_1 + S_2$ values ranged from 0.2217 to 1.0163 mg/g, with an average of 0.5494 mg/g, with good potential for hydrocarbon production.

4.2. Mineral Composition Characteristics. The mineral composition of the shale samples in Table 2 can be divided into clay minerals, brittle minerals, and other minerals (pyrite, etc.), with the content of clay minerals ranging from 32.8% to 76.7%, with an average of 57.4%; brittle minerals ranging from 23.3% to 67.2%, with an average of 42.6%; and pyrite ranging from 2.4% to 3.8%, with an average of 3.1%.

There are many types of clay minerals and brittle minerals. The content of illite in clay minerals ranges from 20.7% to 70%, with an average of 39.3%; the content of kaolinite ranges from 16.2% to 100%, with an average of 62.2%; the content of chlorite ranges from 13.3% to 13.8%, with an average of 13.6%. The content of quartz in the brittle minerals ranged from 23.3% to 64.1%, with an average of 41.6%, and the content of oblique feldspar in samples Y1-9 was 3.1%. The mineral content of shale samples varies greatly with depth (Figure 3). The mineral content of clay in the Lower Shihezi group (Y1-8 and Y1-9) ranges from 32.8% to 67.0%, with an average of 49.9%; the mineral content of quartz ranges from 33.0% to 64.1%, with an average of 48.55%. The content of clay minerals in the Shanxi group (Y1-16, Y1-18) ranged from 61.4% to 76.7%, with an average of 69.05%; the content of quartz ranged from 23.3% to 38.6%, with an average of 30.95%. The clay mineral content of the Taiyuan group (Y1-36, Y1-42, Y1-44, Y1-47) ranged from 43.4% to 70.4%, with an average of 55.3%; the quartz content ranged from 28.8% to 56.7%, with an average of 44.0%. The quartz content was larger in the upper part of the shale reservoir, and the total clay minerals were larger in the lower part of the reservoir.

4.3. Pore Fracture Structure Characteristics

4.3.1. Qualitative-Semiquantitative Characterization. Loucks [23] et al. provide a simple and objective classification of pores associated with the mudstone matrix, including three basic types: (1) pores between particles and crystals, (2) pores within mineral particles, and (3) pores within organic matter. Based on SEM, the development status of different types of pores and fractures in shale can be obtained, and the pore fracture parameters can be obtained semiquantitatively (Figure 4).

Table 1: Geochemical parameters of shale gas reservoir samples from Lower Shihezi group to Taiyuan group in Y1 well.

Sample No.	Sampling level	Sampling depth /m	Lithologic	TOC /%	Organic matter type	R_o/%	T_{max}/°C	$(S_1 + S_2)$ /(mg/g)
Y1-5	Lower Shihezi group	1394.09	Sandy mudstone	0.67	Type III	1.85	478.09	0.359
Y1-8	Lower Shihezi group	1414.7	Siltstone	0.73	Type III	1.71	469.34	0.2217
Y1-30	Taiyuan group	1486	Sandy mudstone	2.07	Type III	1.84	489.76	0.7513
Y1-39	Taiyuan group	1523.1	Siltstone	1.2	Type III		473.51	0.4404
Y1-45	Taiyuan group	1540.15	Mudstone	0.71	Type III	1.94	478.09	0.276
Y1-46	Taiyuan group	1543.7	Siltstone	2.75	Type III		483.51	0.7809
Y1-50	Taiyuan group	1558.2	Sandy mudstone	2.68	Type III	2.10	490.17	1.0163

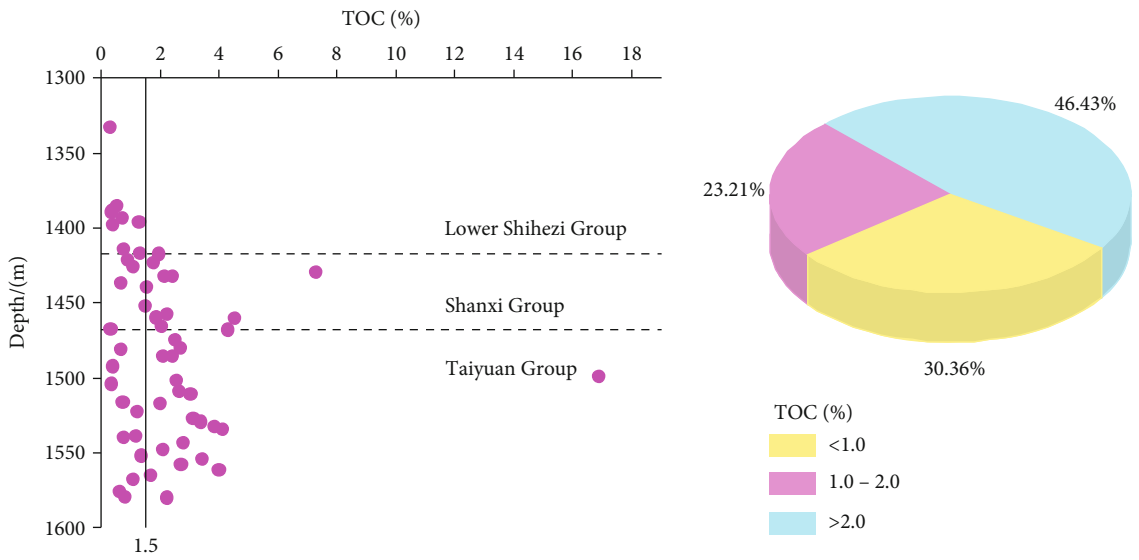

Figure 2: TOC content and percentage of Lower Shihezi Group to Taiyuan Group in Y1 well.

Table 2: Mineral composition content of shale gas reservoir in the Lower Shihezi group to the Taiyuan group of well Y1.

Sample No.	Mineral content/%					
	Quartz	Plagioclase	Pyrite	Sphalerite	Plaster	Total clay
Y1-8	33.0					67.0
Y1-9	64.1	3.1				32.8
Y1-16	23.3					76.7
Y1-18	38.6					61.4
Y1-36	46.5		3.8			49.7
Y1-42	28.8		2.4	11.0		57.8
Y1-44					29.6	70.4
Y1-47	56.7					43.3

Intergranular pores: intergranular pores are generally triangular and elongated in cross-section between larger clay flake crystals Figures 4(a) and 4(i). Intergranular pores are usually present between clay and mineral particles or between ductile clay and rigid particles, but also between clay aggregates that may be compacted clay flocs. Intergranular pores are more abundant in young or shallowly buried sediments and are well connected, forming an effective network of pores between each other.

Intragranular pores: intragranular pores are pores within mineral grains, most of which are within the grains, but intergranular pores are also common locally. Some of the pores in the intragranular pores are primary, and most may have formed during rock formation. Intragranular pores include brittle mineral dissolution pores, clay mineral intragranular pores, and pyrite cast film pores (Figures 4(c), 4(d), and 4(k)). Intragranular pores are usually isolated and poorly connected.

Organic pores: organic pores are intragranular pores within the organic matter, the formation of which is closely related to the evolution of organic matter. Organic pore shapes have irregular, pitted, elliptical cross-sections (Figures 4(b) and 4(l)), usually between 5 and 750 nm in length, and exhibit connectivity in three-dimensional space.

Microcracks: in addition to pores, a large number of microcracks are developed in the shale samples. They are mainly located within the organic material and at the edges of organic and clay mineral grains, such as the clay mineral interbedded fissures (Figure 4(j)). These nonbasal pores are

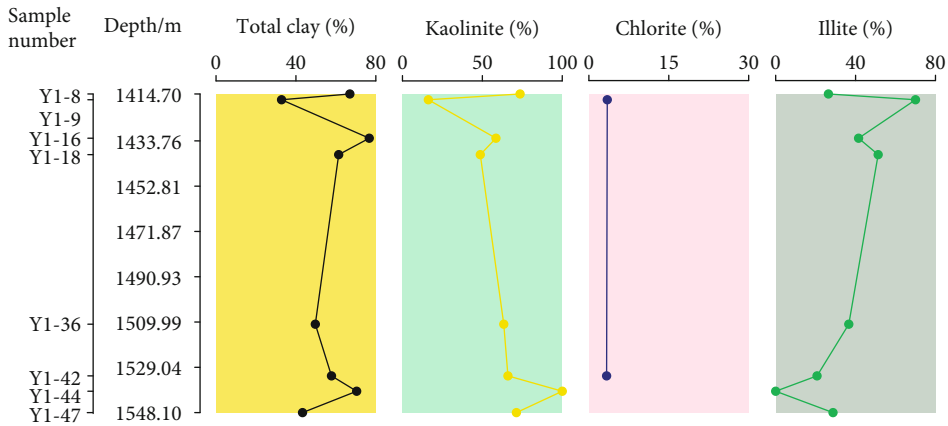

Figure 3: Mineral content of shale reservoir in the Lower Shihezi Formation to Taiyuan Formation of well Y1.

very important in shale gas systems, and their presence and incomplete cementation can have a significant impact on oil and gas production.

4.3.2. Quantitative Characterization

(1) Fractal Theory and Model of 2D SEM Image. For the self-similarity of objects, the French mathematician Mandelbrot [24] introduced the concept of fractal geometric dimensionality to quantitatively characterize the degree of irregularity of an object's surface. The basic principle is that, assuming A is a bounded set in an n-dimensional Euclidean space, if A can be represented as a subset of Nr that mutually uncovered subsets of itself, then A has self-similarity, and the fractal dimension D of A is represented by Eq. (1).

$$D = \frac{\log(N_r)}{\log(1/r)}, \tag{1}$$

where r is the scale factor in the coordinate direction, and N_r is a mutually uncovered subset of the bounded set A.

Zhang et al. [25] argue that the variation of image grayscale indicates the roughness of the object surface, and its fractal dimension can be obtained by measuring the image surface at different scales. SEM images of mud shale reservoirs can be extracted and quantitatively analyzed using IPP software [26] (Figures 4(e)–(h)), combined with fractal theory, to obtain fractal dimensions of different pores. Based on the fractal characteristics of the two-dimensional images of the coal reservoir pore fractures, Pan et al. [27] proposed to represent them in a double logarithmic form (Eq. (2))).

$$1\mathrm{nR} = \frac{\beta}{2}1\mathrm{nA} + C, \tag{2}$$

where $\beta/2$ represents the slope of the linear fit of LnR to LnA, and C is a constant. The fractal dimension of pore fracture morphology in SEM images of mud shale reservoirs is $D = 3 - \beta/2$ according to Pan et al. In addition, the roundness (r) is also a shape factor reflecting the pore roughness [28, 29], and the expression (3) is

$$r = 4A/\pi R^2 \tag{3}$$

(2) Fractal Characteristics of Pore Fracture Morphology. The pore length axis and area data in SEM images of different mud shale pore types were used for mapping, and it can be seen that LnA and LnR in Figure 5 show obvious linear relationship, and the coefficient of fit (R^2) is greater than 0.86, which indicates that the shale reservoir pore fracture morphology has good fractal characteristics. The fractal dimension and roundness of shale reservoir pore fracture morphology are calculated based on Eqs. (2)) and (3), and the results are shown in Table 3.

Based on the fractal theory, the fractal dimension of a geometric polyhedron in n-dimensional space should satisfy $n - 1 < D < n + 1$, and thus the fractal dimension of the three-dimensional pores in shale samples should satisfy $2 < D < 3$ [30]. The fractal dimension of pore fractures (D_{SEM}) in shale reservoirs ranges from 2.34 to 2.50, and the pore roundness (r) is between 0.58 and 0.79. Liu et al. [31] concluded that the closer the fractal dimension D is to 3.0, the less smooth the solid pores are indicated; conversely, when the fractal dimension D is closer to 2.0, the smoother the pore surface is. In addition, the roundness of the pores is greater than 0.58, indicating that the shape of the pores in the shale is regular and simple.

(3) Quantitative Porosity Characterization. According to the IUPAC classification scheme, the pores are classified into three types according to the pore diameter as macroporous (>50 nm), mesoporous (2 ~ 50 nm), and microporous (<2 nm) [32].In this paper, high-pressure pressure mercury and low-temperature nitrogen adsorption experiments are used to characterize the pore structure of the macroporous and mesoporous pores of the Y1 well shale samples, and the results are shown in Table 4.

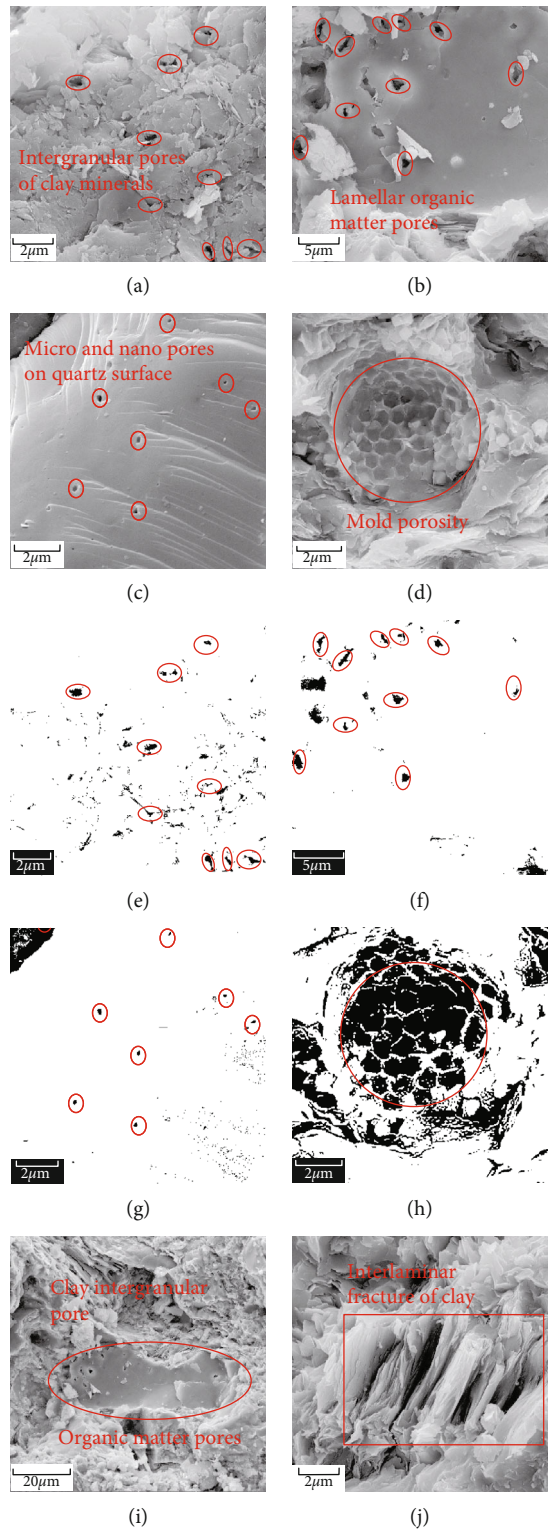

Figure 4: Continued.

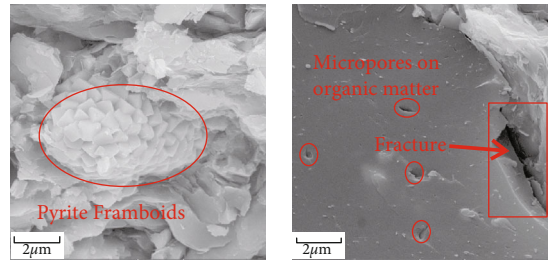

(k) (l)

Figure 4: Pore types of shale gas reservoir in the Lower Shihezi group to the Taiyuan group of well Y1.

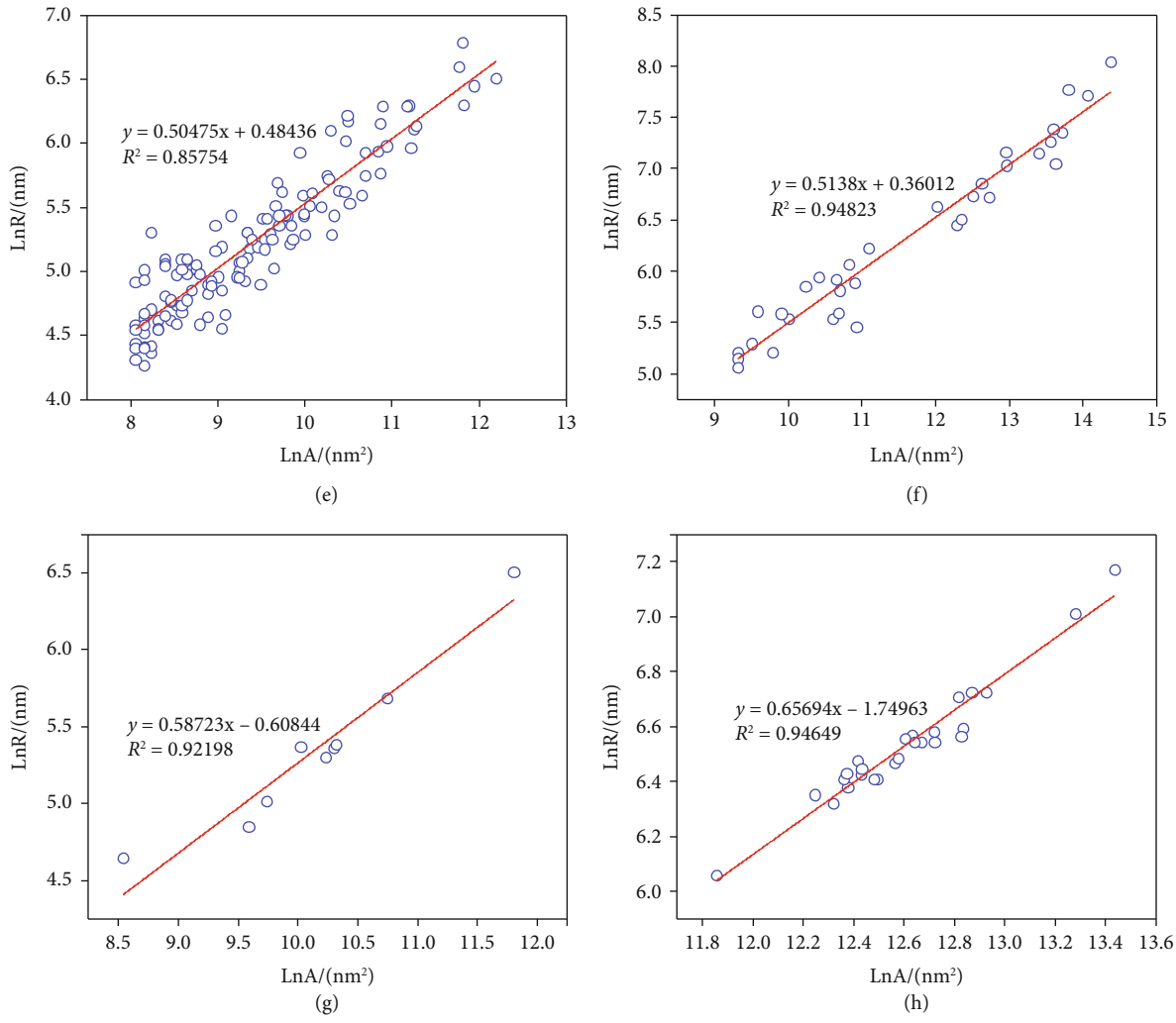

Figure 5: Double logarithmic curves of pore long axis and area in SEM images of shale with different pore types in well Y1.

The results of mercury pressure experiment show that the pore size of shale samples in well Y1 is between 17.88 nm and 9095 nm, with an average value of 1340 nm, a specific pore volume of 0.0037-0.0162 cm^3/g, an average value of 0.008457 cm^3/g, a specific surface area of 0.0021-2.8058 m^2/g, an average value of 0.856057 m^2/g, and a total porosity of 0.974%-3.9976%, with an average value of 2.161%. The results of low-temperature nitrogen adsorption experiment show that the pore size of mesoporous is between 6.641249 and 26.886218 nm, the average value is 10.9231 nm, the BET specific surface area is between 2.137808 and 12.442336 m^2/g, the average value is 7.594496 m^2/g, the total pore volume is between 0.011809 and 0.021441 cm^3/g, and the average value is 0.016804 cm^3/g.

The high-pressure mercury pore size analysis method uses high pressure to inject mercury into the pores of shale

Table 3: Pore parameters and fractal dimension extracted from SEM images of Well Y1.

Pore type	Average pore area/nm^2	Pore long axis/nm	Average pore size/nm	Roundness r	Fractal dimension D_{SEM}	Coefficient of fit R^2
e	21970.87	220.2492	151.6757	0.576964	2.49525	0.85754
f	321437.6	796.5479	532.6897	0.645362	2.4862	0.94823
g	36296.67	243.73	188.1144	0.778358	2.41277	0.92198
h	271345	682.0643	568.4628	0.743022	2.34306	0.94649

Table 4: Pore structure parameters of high-pressure mercury injection and low-temperature liquid nitrogen adsorption experiment in well Y1.

Sample No.	High-pressure mercury pore structure parameters				Cryogenic liquid nitrogen pore structure parameters		
	Average pore size (nm)	Specific pore volume (cm^3/g)	Specific surface area (m^2/g)	Porosity (%)	Average pore size (nm)	Total pore volume (cm^3/g)	BET surface area (m^2/g)
Y1-4	17.88	0.013	2.8058	3.3503	7.77312	0.018128	9.328797
Y1-7	26.34	0.0053	0.7688	1.3977	9.569508	0.021441	8.962331
Y1-20	9095	0.006	0.0021	1.5052	9.087332	0.015925	7.009854
Y1-26	26.9	0.0103	1.4364	2.6505	6.641249	0.020658	12.442336
Y1-27	74.54	0.0162	0.7726	3.9976	9.77518	0.015299	6.260349
Y1-38	28.75	0.0037	0.0497	0.974	26.886218	0.014369	2.137808
Y1-49	114.7	0.0047	0.157	1.2517	6.729061	0.011809	7.019995

and obtains the internal pore size and distribution by measuring the pore size curve and the drainage pressure. The mercury intrusion method is a standard method to obtain the micronnanoscale pore distribution characteristics.

Based on the mercury intrusion experiments, the coal rocks diameter and the mercury inlet pressure satisfy the Washburn equation, namely,

$$r_i = -2\sigma \cos\theta / P_i, \quad (4)$$

where σ is the pore surface tension, J/m^2; θ is the contact angle between mercury vapor and the pore surface of the coal; P_i is the experiment mercury inlet pressure, MPa; and r_i is the experimentally measured pore size by the mercury inlet pressure P_i, μm.

(1) The sample entry/exit curves are shown in Figure 6, which are divided into three categories according to the type and characteristics of the curves.

The first type of curve is shown in Figure 6 for sample Y1-4. Compared with other samples, the mercury inlet curve is obviously rising rapidly, indicating that there are a large number of large pores in the sample. The mercury removal curve first rises sharply and then becomes horizontal, indicating that the micropores and mesopores are also relatively developed. The type of pores is dominated by ink bottle pores. The "hysteresis ring" has a large volume, indicating that most of the pores are open pores, and the pore connectivity is excellent. The pore structure is conducive to shale gas desorption and seepage and diffusion.

The second type of curve is sample Y1-26 in Figure 4. When the pressure is less than 50 MPa, the mercury inlet curve is smoother, indicating that the pore throats and corresponding macropores are developed at this time. When the pressure is greater than 50 MPa, the mercury inlet curve rises sharply. The curve is not smooth, and the pore throats and corresponding pores are poorly sorted. The mercury removal curve first slowly rises horizontally, and then upwardly convex, indicating that a large number of mesopores and micropores are developed at this time, and the pore types are predominantly of the slit type, the amount of mercury removal is small, and the "hysteresis ring" is wider, indicating that the sample has more open pores and better pore connectivity, which is also conducive to the desorption, seepage, and diffusion of shale gas.

The third type of curve is shown in Figure 4 for sample Y1-7 and sample Y1-27. The volume difference between the advancing and retreating mercury curves is small, and the "hysteresis loop" is narrow, indicating that semiclosed pores and dead pores are mostly developed in the sample, and the pore connectivity is poor. The pore structure is extremely unfavorable for shale gas desorption, seepage, and diffusion.

(2) The pore size distribution curve of mercury injection in shale samples is shown in Figure 7. The pore size range of high-pressure mercury injection test is 3 ~ 200000 nm, and the pore size range is between transition pore and macropore. The test results can be used to characterize the pore size distribution. The decimal classification scheme [32] was introduced: micropore < 10 nm, transition pore 10~100 nm, mesopore 100~1000 nm, and macropore>1000 nm

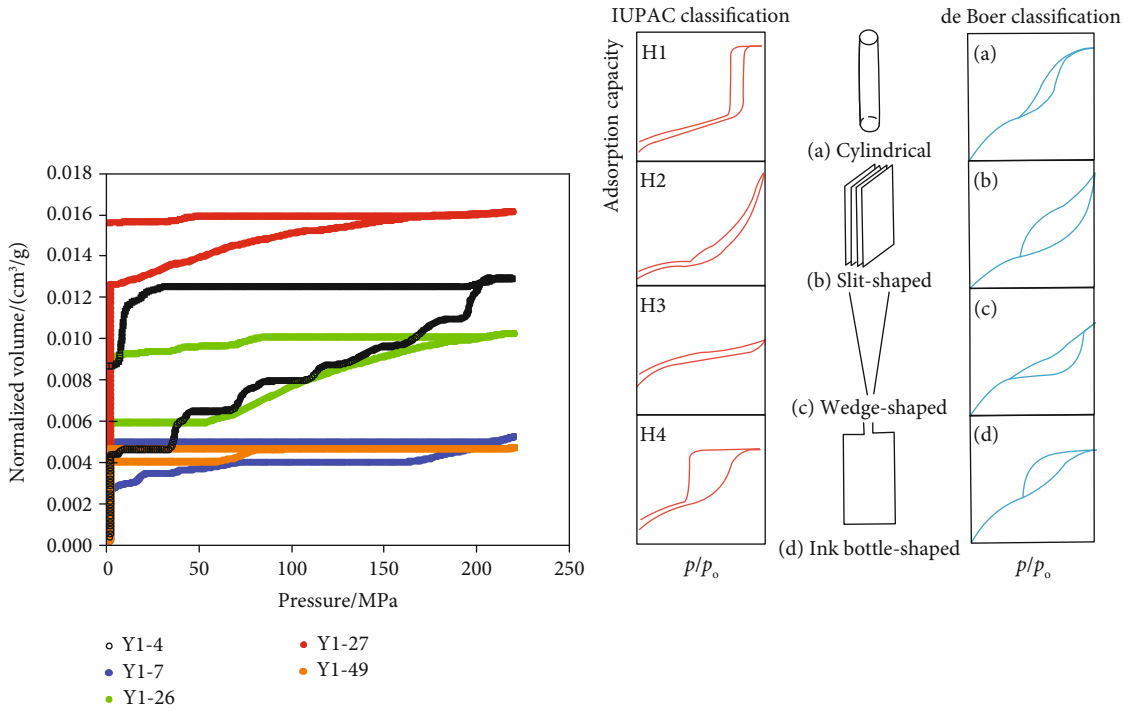

Figure 6: Mercury advance and retreat curve and corresponding pore types of samples from well Y1 [11] [31].

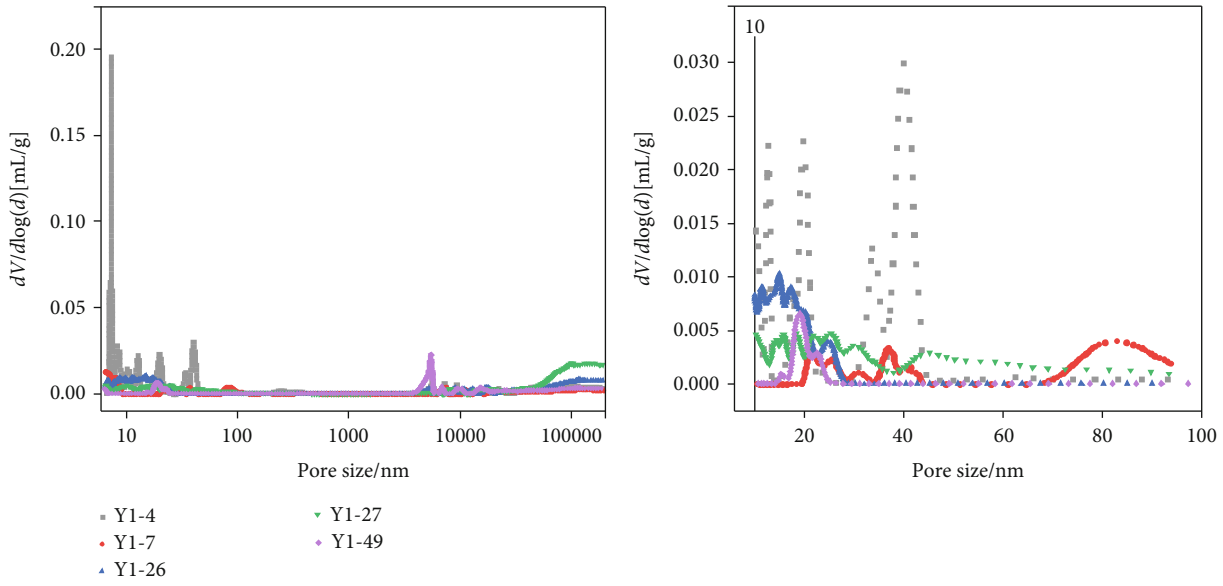

Figure 7: Pore size distribution of shale samples.

Figure 7 shows the dV/dW pore size distribution curves of shale samples from some drill cores in the study area. The pore sizes of shale samples from well Y1 in the study area are mainly located in some transitional pore sections and large pore sections, with no medium pore sections, and the overall pores smaller than about 1000 nm are the main pore sizes. According to the differential pore volume to pore size distribution curves, the shale samples can be divided into two categories: (1) samples Y1-4 and Y1-49, which have a bimodal pattern of primary and secondary pore sizes, with the absolute dominance of large pores. (2) Samples Y1-7, Y1-26, and Y1-27, which have no mesopore peaks, have a broad and slow pore size distribution with multiple peaks and have higher organic matter abundance than other shale samples. The abundance of organic matter is higher than other shale samples. At the same time, sample Y1-4 has a steep mercury feed curve in the 10-100 nm region, indicating that the pore size distribution is concentrated in the transition pore region, which is the dominant pore size section. Similarly, Y1-49 is in the 5000 nm-6000 band. In general,

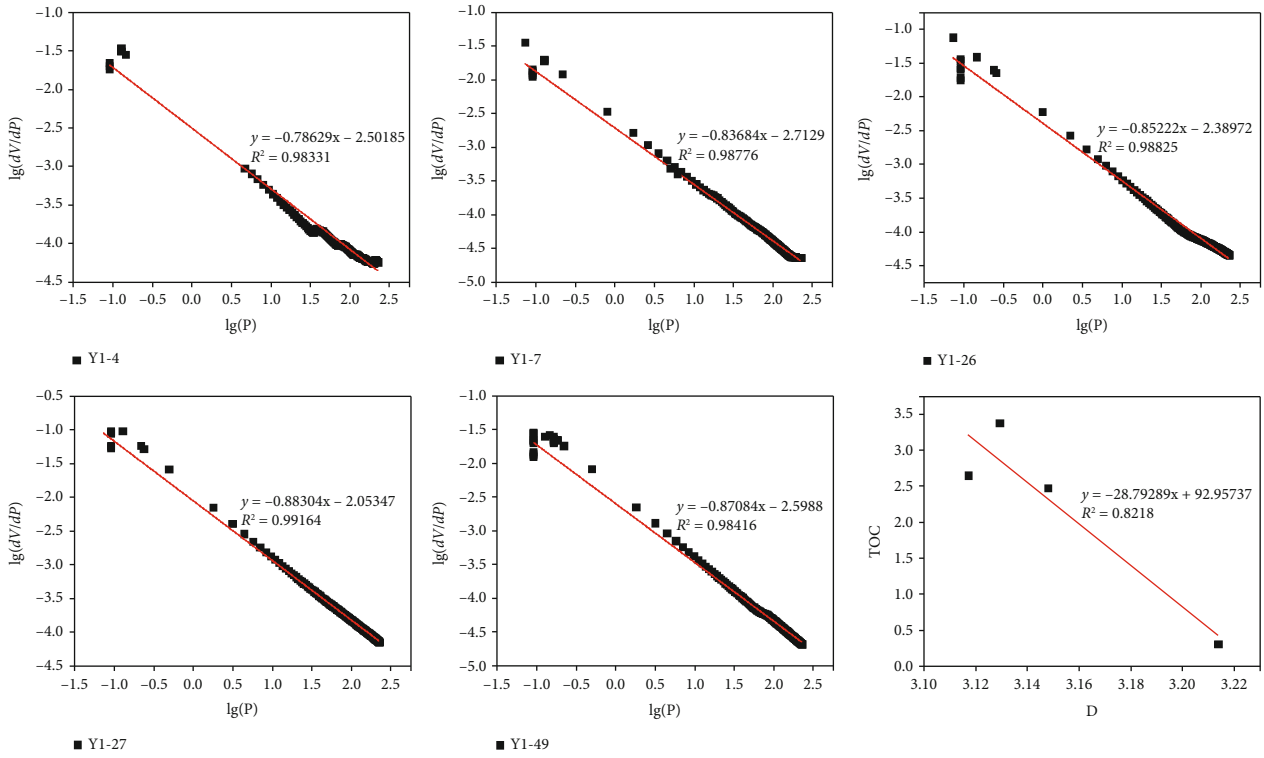

Figure 8: Fractal characteristics of pores in mercury injection experiments and the relationship between TOC and fractal dimension.

the organic matter and clay minerals in the shale samples provide a large number of micropore-macropore pores, which form a complex pore network.

(4) Fractal Theory and Model of Percolation Pores. According to the fractal theory of the sponge structure, the double logarithmic relationship between the cumulative mercury volume and the coal pore size was established. The relationship is.

$$\log (dV_i/dr_i) \propto (2\text{-}D) \log (r_i), \tag{5}$$

where V_i is the cumulative mercury volume, cm^3/g; D is the fractal dimension. Combining Eqs. (4) and (5) can obtain the relationship between the pore fractal dimension, the mercury inlet pressure, and the cumulative mercury inlet volume, namely,

$$\log (dV_i/dP_i) \propto (D\text{-}4) \log (P_i). \tag{6}$$

The slope K was obtained by linear fitting $\log(dV_i/dP_i)$ and $\log(dP_i)$. Then, the fractal dimension D can be expressed as $D = K + 4$.

The relationship between $\log(dV_i/dP_i)$ and $\log(dP_i)$ was obtained according to Eqs. (3)–(6) (Figure 8), and the pore pore fractal dimension D of each shale sample was 3.11696 to 3.21371 with a mean value of 3.154154. According to the fractal theory, the branching dimension of porous solid pores is between 2 and 3, while the fractal dimension D of pore pore samples in the eastern margin of Ordos Basin is greater than 3, and it can be seen from Figure 7 that each shale has a higher fit ratio (R^2 is greater than 0.98). And the fractal dimension D of the percolation pore has a high correlation with the TOC content.

4.4. Gas Content Characteristics

4.4.1. Isothermal Adsorption Characteristics. The gas adsorption capacity of shale reservoirs determines the size of its reserves. Based on the isotherm adsorption experiment, this paper uses the Langmuir model to characterize the gas adsorption capacity of the Lower Shihezi group, Shanxi group, and Taiyuan group shale in the Y1 well, and the isothermal adsorption of the shale samples was calculated according to Langmuir's isothermal equation (7). The Langmuir adsorption isotherm is

$$V = \frac{VLp}{p + pL}, \tag{7}$$

where V is the amount of gas adsorbed by the shale at a gas pressure of p, V_L is the Langmuir volume, and p_L is the Langmuir pressure.

The results show that the maximum adsorption capacity of the four shale samples is 0.6758 cm^3/g, the Y1-4 content is too low and gradually decreases in the vertical direction, which is all lower than the isotherm adsorption capacity of marine shale in China (1.73~3.28 cm^3/g). Among them, the TOC content has a good correlation with Lang's volume ($R^2 = 0.53$) (Figure 9).

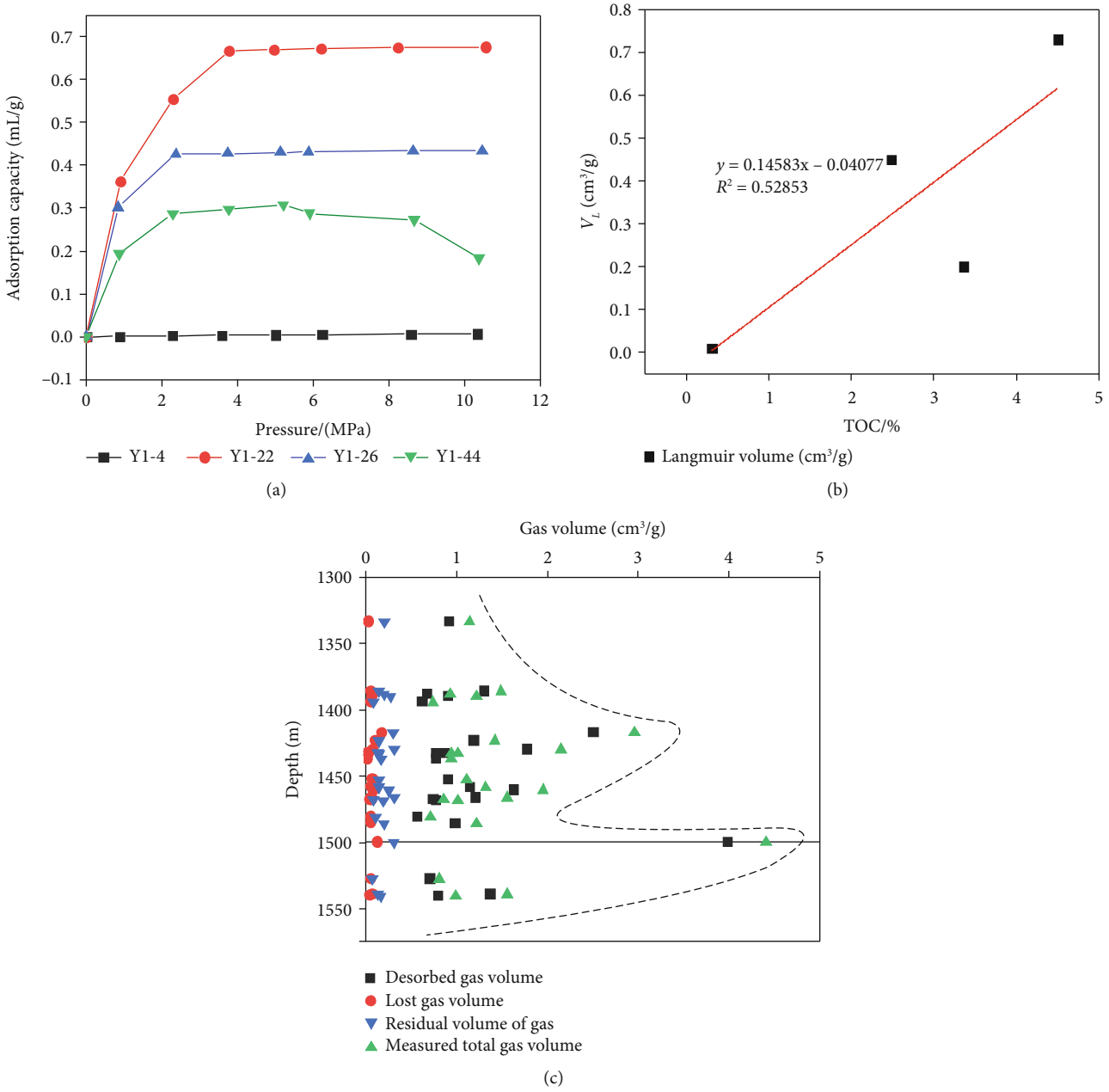

Figure 9: CH4 isothermal adsorption curve and vertical gas content change curve of well Y1.

4.4.2. Measured Gas Content. The gas content of the shale samples from Y1 well showed that the desorption volume ranged from 0.5593 to 3.9820 cm^3/g, with a mean value of 1.1720 cm^3/g; the loss volume ranged from 0.0125 to 0.1629 cm^3/g, with a mean value of 0.0564 cm^3/g; the residual gas volume ranged from 0.0666 to 0.3120 cm^3/g, with a mean value of 0.1825 cm^3/g; the measured total gas content ranges from 0.71 to 4.41 cm^3/g, with an average value of 1.4109 cm^3/g. Longitudinally, the gas content in the contact section between the Shanxi group and Taiyuan group is higher, decreasing from the Taiyuan group and increasing again at 1499 m depth, reaching a maximum value of 4.41 cm^3/g. The vast majority of the samples have a total gas content greater than the lower limit of 0.5 cm^3/g for industrial shale gas development [33]; so, the Y1 well shale reservoir has some exploration potential (Figure 9).

5. Discussions

5.1. Factors Influencing the Development of Pore Structures. Pore volume and specific surface area are the main parameters for evaluating shale gas reservoirs, and in this paper, the geochemical parameters and main mineral content of mud shale reservoirs are used as variables to discuss their correlation with different pore size pores.

5.1.1. Relationship between Geochemical Parameters and Pore Structure Parameters. The results in Figure 10 show that the

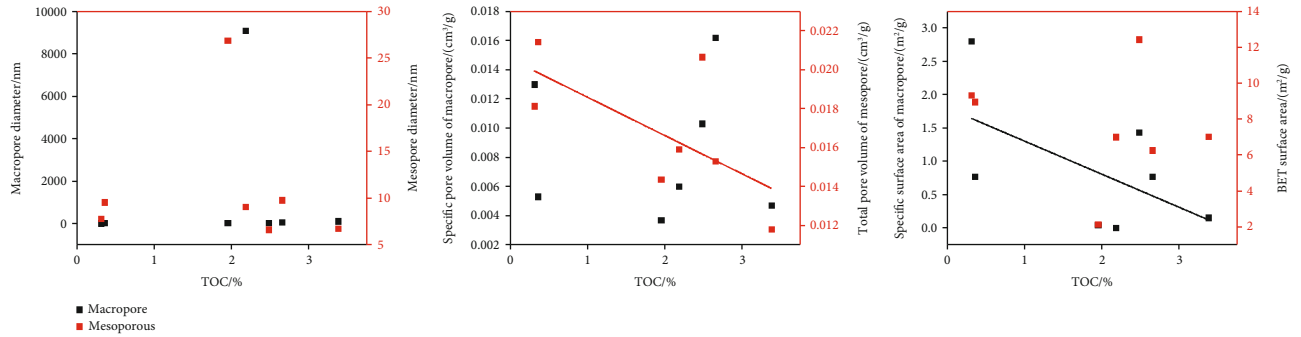

Figure 10: Relationship between geochemical parameters and pore structure parameters of shale samples.

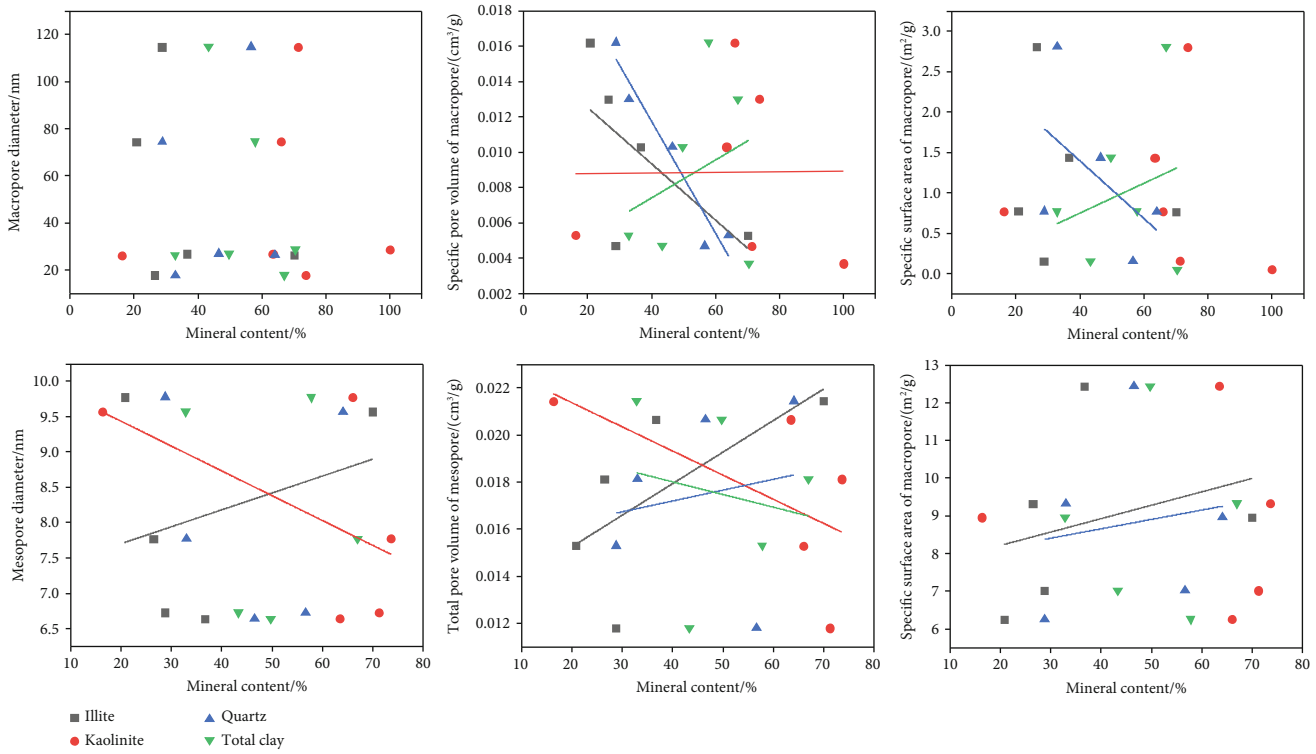

Figure 11: Relationship between main mineral composition and pore structure parameters of shale sample.

TOC content has no significant linear relationship with the pore size of both macro and mesopores, a slight negative correlation with the mesopore pore volume and macroporous specific surface area, and an insignificant correlation with the macroporous pore volume and mesopore specific surface area. The analysis is due to the thermal evolution of the organic matter, which generates a large number of nanoscale pores within the organic matter; and some of the larger mesopores and macroporous pores are filled by later debris material. In addition, R_o and pore structure parameters are not discussed in relation to each other because the samples taken in this study area have similar degree of thermal evolution and small span of maturation intervals.

5.1.2. Relationship between Main Mineral Composition and Pore Structure Parameters. The mineral composition of the Y1 well shale samples is shown in Table 2 and can be generally divided into three main categories: brittle minerals, clay minerals, and other minerals. As shown in Figure 11, macroporous pore volume and specific surface area show a linear positive correlation with the total clay content and a linear negative correlation with the content of brittle minerals (quartz), and the correlation between mesopore pore volume and specific surface area and the total clay content is not too obvious. The reason for this is mainly the poor development of micromesopores within the quartz, where the pore volume and specific surface area are mainly contributed by the intergranular pores of brittle mineral grains with larger pore sizes. The sample mesopore aperture and pore volume showed a linear positive correlation with the content of illite and a linear negative correlation with the content of kaolinite; the correlation between macroporous aperture and clay mineral

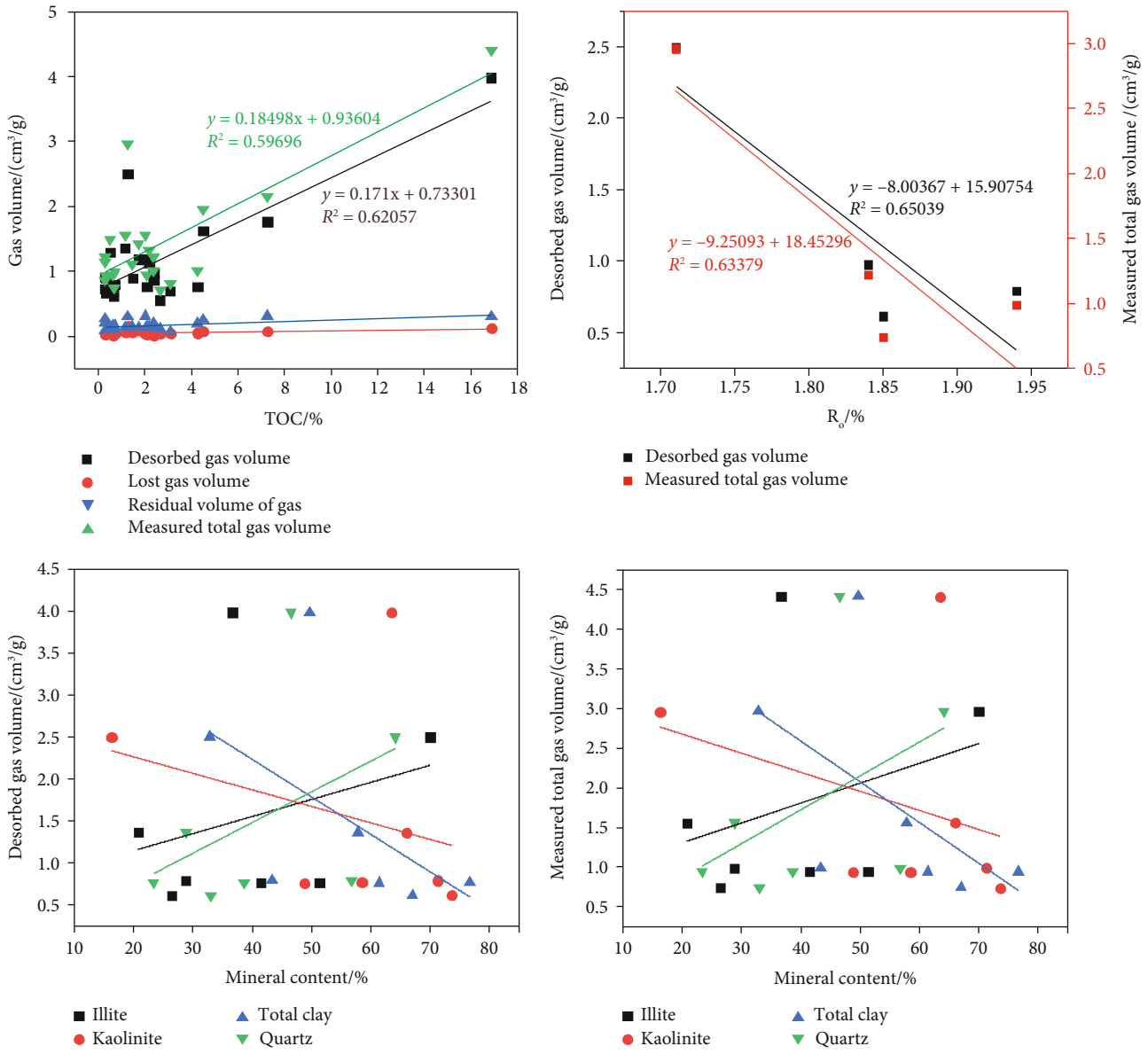

Figure 12: Effects of shale geochemical parameters and different components on gas content.

composition was not obvious, and macroporous aperture volume showed a linear negative correlation with the content of illite and quartz, respectively, which was analyzed to be due to the differences in the structure of different clay minerals.

5.2. Factors Influencing the Gas-Bearing Properties of Shale Reservoirs. The analysis of the gas content of the shale reservoir from the geochemical parameters and the main material composition of the samples showed that the TOC content, desorption, and total gas content had a certain positive correlation, while the R_o showed an obvious negative correlation with desorption and total gas content, with the correlation coefficients of $R^2 = 0.65$ and $R^2 = 0.63$, respectively, which indicated that the abundance of organic matter and the degree of thermal evolution had a certain positive correlation with the gas content of the shale reservoir plays a key role (Figure 12). Kaolinite has some negative correlation with desorption and total gas content, while illite is mostly positively correlated with desorption and gas content, but on the whole, clay minerals are negatively correlated with desorption and total gas content (Figure 12). The clay minerals are mainly composed of two basic units, silica-oxytetrahedra and aluminoxo-octahedra, and illite is more well developed than the kaolinite interbedded structure and internal surface area. Quartz is one of the main minerals that make up the shale, probably due to its stable crystal structure, which increases the intergranular pores with other materials, resulting in an increase in the specific surface area and specific pore capacity of the pores, and therefore, the quartz content is significantly positively correlated with both desorption and total gas content (Figure 12).

6. Conclusions

(1) The organic matter type of well Y1 in Ordos Basin is type III, with the TOC content ranging from 0.28% to 16.87%, with an average of 2.15%; R_o is 2.45%-3.36%, with an average of 2.86%. Hydrocarbon generation potential is objective

(2) The pore types of marine-continental transitional shale in well Y1 include mineral pores and organic matter pores, and the former includes mineral intergranular pores, mineral intergranular pores, cast membrane pores, and other mineral intragranular pores. The intergranular pores and organic pores of lamellar clay minerals are widely developed in the marine-continental transitional shale. Shale pore fracture morphology heterogeneity is moderate, controlled by the pore structure

(3) In Y1 well, there are many open pores, including parallel plate-shaped pores and wedge-shaped pores, but few ink bottle pores and semiclosed pores. The BET-pecific surface area ranged from 2.137808 to 12.442336 m^2/g, and total pore volume ranged from 0.011809 to 0.021441 cm^3/g, with an average of 0.016804 cm^3/g. The pore size of shale samples is mainly located in the transitional and macroporous sections, with no mesoporous sections, and the main pore diameters are pores less than 1000 nm

(4) The controlling factors of pore development of marine-continental transitional shale in well Y1 are complex. TOC content, clay mineral, and quartz content are the main factors of pore development. The results show that pore volume and specific surface area are positively correlated with clay mineral content, TOC, and overall, but negatively correlated with the quartz content; the illite content in clay minerals has a positive effect, and the kaolinite content is not conducive to the development of pore volume and specific surface area; quartz is an unfavorable factor in brittle minerals, which has a greater influence; the measured total gas content and desorption gas volume have a significant positive correlation with TOC. There is a weak positive correlation with the content of quartz and illite

Data Availability

The data can be found in the National Earth System Science Data Sharing Infrastructure in China.

Conflicts of Interest

The author(s) declare(s) that they have no conflicts of interest.

Authors' Contributions

Yuanzhen Ma and Meng Wang conceived and designed the schemes. Yuanzhen Ma and Ruying Ma collected the samples. Yuanzhen Ma, Ruying Ma, Jiamin Li, and Asiya Bake performed the experiments. Yuanzhen Ma analyzed the data and wrote the manuscript.

Acknowledgments

The authors are sincerely thankful for the Natural Science Foundation of Xinjiang (grant no. 2018D01C062), the Fundamental Research Funds for the Central Universities (No. 2020ZDPYMS09), and the NSFC-Xinjiang Joint Fund (No. U1903209).

References

[1] H. D. Chen, J. Li, and C. G. Zhang, "Discussion of sedimentary environment and its geological enlightenment of Shanxi formation in Ordos Basin," *Acta Petrologica Sinica*, vol. 27, no. 8, pp. 2213–2229, 2011.

[2] W. L. Yang, Y. Wang, and Y. P. Sun, "Gas potential of the Upper Paleozoic in the southern Ordos Basin," *Natural Gas Industry*, vol. 29, no. 12, 2009.

[3] J. H. Fu, S. B. Guo, and X. S. Liu, "Shale gas accumulation condition and exploration potential of the upper Paleozoic Shanxi formation in Ordos Basin," *Journal of Jilin University (Earth Science Edition)*, vol. 43, no. 2, pp. 382–389, 2013.

[4] M. L. Gong, W. L. Ding, and D. D. Pi, "Forming conditions of shale gas of the Shanxi formation of Permian in the southeast of Ordos Basin," *Journal of Northeast Petroleum University*, vol. 37, no. 3, 2013.

[5] S. B. Guo, J. J. Fu, and D. Gao, "Research status and prospects for marine-continental shale gases in China," *Petroleum Geology and Experiment*, vol. 37, no. 5, pp. 535–540, 2015.

[6] J. Y. Gu, J. P. Ye, and C. Fang, "Prospects of shale gas resources in Qinshui Basin," in *Proceedings of the 2011 Coalbed methane symposium*, Beijing: Geological Publishing House, 2011.

[7] S. H. Tang, E. P. Fan, and S. H. Zhang, "Reservoir characteristics and gas-bearing capacity of the lower Palaeozoic marine shales in northwestern Hunan," *Earth Science Frontiers*, vol. 23, no. 2, pp. 135–146, 2016.

[8] J. Z. Zhang, X. Q. Li, and Y. Liu, "Characteristics and gas-bearing analysis of marine shale reservoirs in the lower Paleozoic in northwestern Hunan," *Coal Geology of China*, vol. 26, no. 12, pp. 1–6, 2014.

[9] Y. P. Chen, W. H. Huang, and X. X. Lu, "Shale gas reservoir-forming conditions in Qinshui basin's marine-continental facies," *Resources & Industries*, vol. 15, no. 3, pp. 68–72, 2013.

[10] C. Yang, J. C. Zhang, and X. Tang, "Microscopic pore types and its impact on the storage and permeability of continental shale gas," *Ordos Basin Earth Science Frontiers*, vol. 20, no. 4, pp. 240–250, 2013.

[11] Z. B. Tian, S. H. Wei, and J. Q. Wang, "Et el. Characteristics of microscale pore structures of marine-continental transitional shale from the mid-eastern area, Qinshui Basin," *Journal of China Coal Society*, vol. 42, no. 7, pp. 1818–1827, 2017.

[12] S. B. Guo and L. Huang, "Gas-bearing influential factors and evaluation of shale gas reservoir: a case study of Paleozoic shale gas reservoir in upper Yangtze region," *Petroleum Geology and Experiment*, vol. 35, no. 6, pp. 601–606, 2013.

[13] S. B. Guo and K. Y. Zhao, "Gas-bearing influential factors and estimation of shale reservoirs in Upper Paleozoic, Ordos Basin," *Petroleum Geology and Experiment*, vol. 36, no. 6, 2014.

[14] D. L. Xie, Y. H. Guo, and D. F. Zhao, "Fractal characteristics of adsorption pore of shale based on low temperature nitrogen experiment," *Journal of China Coal Society*, vol. 39, no. 12, pp. 2466–2472, 2014.

[15] F. Yang, Z. F. Ning, and H. Q. Liu, "Fractal characteristics of shales from a shale gas reservoir in the Sichuan Basin, China," *Fuel*, vol. 115, pp. 378–384, 2014.

[16] F. Yang, Z. F. Ning, and Q. Wang, "Fractal characteristics of nanopore in shales," *Natural Gas Geoscience*, vol. 25, no. 4, pp. 618–623, 2014.

[17] T. T. Cao, Z. G. Song, and H. Y. Luo, "Pore system characteristics of Permian transitional shale reservoir in the lower Yangtze region, China," *Natural Gas Geoscience*, vol. 27, no. 7, pp. 1332–1345, 2016.

[18] X. Tang, J. C. Zhang, and W. L. Ding, "The reservoir property of the upper Paleozoic marine-continental transitional shale and its gas-bearing capacity in the southeastern Ordos Basin," *Earth Science Frontiers*, vol. 23, no. 2, pp. 147–157, 2016.

[19] X. G. Dai and M. Wang, "Shale reservoir properties and gas-bearing properties of marine-continental shale in Ordos Basin," *Science Technology and Engineering*, vol. 17, no. 15, pp. 26–32, 2017.

[20] W. D. Xie, M. Wang, and X. G. Dai, "Microscopic characteristics of shale gas reservoirs in middle and southern coal measures of Hedong coalfield, Shanxi Province," *Natural Gas Geoscience*, vol. 30, no. 4, pp. 515–525, 2019.

[21] R. Y. Ma, M. Wang, W. D. Xie, and H. Wang, "Micro-pore reservoir spaces and gas-bearing characteristics of the shale reservoirs of the coal measure strata in the Qinshui Basin," *Journal of Nanoscience and Nanotechnology*, vol. 21, no. 1, pp. 371–381, 2021.

[22] R. Y. Ma, J. Zhang, and M. Wang, "Micropore characteristics and gas-bearing characteristics of the shale reservoirs in the transitional facies in the Qinshui basin," *Journal of Henan Polytechnic University (Natural Science)*, vol. 1-11, pp. 1673–9787, 2021.

[23] R. G. Loucks, R. M. Reed, S. C. Ruppel, and U. Hammes, "Spectrum of pore types and networks in mud-rocks and a descriptive classification for matrix-related mud-rock pores," *AAPG Bulletin*, vol. 96, no. 6, pp. 1071–1098, 2012.

[24] B. B. Mandelbrot, "Stochastic models for the Earth's relief, the shape and the fractal dimension of the coastlines, and the number-area rule for islands," *Proceedings of the National Academy of Sciences of the United States of America*, vol. 72, no. 10, pp. 3825–3828, 1975.

[25] Z. Zhang, F. Dong, and Y. L. Wu, "Estimation of fractal dimension for 2-D gray image," *Journal of Computer Applications*, vol. 12, 2005.

[26] Z. T. Li, *Evolution of pore-fractures of coal reservoir and its impact on CBM microcosmic flow*, China University of Geoscience (Bei Jing), 2018.

[27] J. N. Pan, K. Wang, Q. L. Hou, Q. Niu, H. Wang, and Z. Ji, "Micro-pores and fractures of coals analysed by field emission scanning electron microscopy and fractal theory," *Fuel*, vol. 164, pp. 277–285, 2016.

[28] P. Soroushian and M. Elzafraney, "Morphological operations, planar mathematical formulations, and stereological interpretations for automated image analysis of concrete microstructure," *Cement and Concrete Composites*, vol. 27, no. 7-8, pp. 823–833, 2005.

[29] G. İ. Sezer, K. Ramyar, B. Karasu, A. B. Göktepe, and A. Sezer, "Image analysis of sulfate attack on hardened cement paste," *Materials Design*, vol. 29, no. 1, pp. 224–231, 2008.

[30] S. H. Zhang, S. H. Tang, and D. Z. Tang, "Fractal characteristics of coal reservoir seepage pore, east margin of Ordos Basin," *Journal of China University of Mining and Technology*, vol. 38, no. 5, pp. 713–718, 2009.

[31] Y. B. Yao and D. M. Liu, *Fine Quantitative Characterization and Comprehensive Evaluation Model of Coal Reservoir*, Geological Publishing House, Beijing, 2013.

[32] D. H. Everett and L. K. Koopal, "International union of pure and applied chemistry," *Polymer*, vol. 31, no. 8, pp. 1598–1598, 2001.

[33] MA RL, *The geological characteristics of the argillutite formation and potentiality for the exploration of the shale gas in Central Hunan,southeastern Hunan and northeastern Hunan*, Chengdu University of Technology, 2013.